An Analytical Study of Single Particle Char Gasification

LUIS ERNESTO ARRI
and
NEAL R. AMUNDSON

Department of Chemical Engineering and Materials Science
University of Minnesota
Minneapolis, Minnesota 55455

The gasification of a single particle of porous char surrounded by a boundary layer with oxygen and water vapor in its environment, taking into consideration the six main reactions along with the appropriate heat and mass transport effects, is considered using a shell-progressive model. Much can be done analytically, and the numerical treatment of the model equations for a variety of parameters elucidates the structure of the problem which is much more complicated than anticipated, in spite of the fact that the model is a relatively simple one. The flame front of burning hydrogen and carbon monoxide can be at the core surface, in the ash layer, or in the boundary layer depending upon the ambient conditions of temperature and oxygen concentration.

SCOPE

Immediately upon attempting to model a gasification reactor, one is faced with the problem of deciding where the various chemical reactions occur. If one considers, for example, the problem of the burning or the gasification of carbon in the presence of water vapor, the minimal set of reactions it makes sense to consider is seven, and these will be discussed later. Even in the simple combustion of an impervious carbon sphere in an atmosphere of oxygen and inert the burning process, as shown recently (Caram and Amundson, 1977), is much more complicated than originally thought. If one envisages such a particle with a boundary layer about it, then the main question to ask is where does the carbon monoxide burn: at the surface of the particle, in the boundary layer, or in the interstitial gas in the reactor. Early workers (Spalding, 1955; van der Held, 1961); and Wicke et al., 1962) considered models essentially too simple, and, therefore, the basic structure of the problem was lost. The answer is indefinite in that the carbon monoxide burns at different places depending upon the prescribed conditions. The more complicated problem of burning a porous carbon sphere has been treated by Wen and Wang (1970), and there is a wealth of material in the literature on gas-solid reactions in general. One can write the transport equations for a porous particle, and one could develop a model which would treat the situation in detail in principle. These would be transient equations, and since all of the reactions are known kinetically more or less well, one could make a parametric study of the gasification of a single particle. This would be an enormous task and probably unnecessary, except as an intellectual and computational exercise. Since the reactions have widely different velocities, and also since the chars have different structures, a substantially less sophisticated analysis should be adequate. Such an analysis is made in this paper. A particle of porous carbon exposed to an atmosphere of oxygen, water vapor, and inert is modeled. This is approximately the situation in the combustion zone of a Lurgi countercurrent gasifier. Early modeling of such a gasifier led the authors to believe that single particle modeling studies should be made in order to determine the possible structure of the solutions. After a great deal of reflection, it seemed that the shell-progressive model, determined primarily by the reaction $C + \frac{1}{2}O_2 = CO$, should be dealt with in detail together with the other reactions of carbon with carbon dioxide, water with carbon, and the water gas shift reaction. The primary purpose of this paper is a study, then, of how a porous carbon sphere with a boundary layer will gasify in the presence of water, oxygen, carbon dioxide, and inert.

CONCLUSIONS AND SIGNIFICANCE

What happens under the above conditions when a shell-progressive model is used for a porous carbon sphere, taking into consideration only those things deemed absolutely essential, cannot be described in simple terms. In the model it is assumed that the core of the shell is a lumped system in which the reactions between carbon, carbon dioxide, carbon monoxide, water, and hydrogen take place, since it is hypothesized that no oxygen proceeds beyond the core surface. Thus, the oxygen diffusing through the ash layer reaches the core surface where it reacts with the carbon core surface and with carbon monoxide and hydrogen produced in the core. This is the case if the ambient oxygen concentration is high enough. If the ambient oxygen concentration is too low, and assuming a core has already been formed, the incoming oxygen will react with the hydrogen and carbon monoxide and, under the assumption that these reactions are instantaneous, will form a flame front at some point outside the core either in the ash layer or in the boundary

Luis Ernesto Arri is with INTEC (U.N.L.–CONICET), Santiago del Estero 2654, 3000 Santa Fé, Argentina. Neal R. Amundson, is with the University of Houston, Houston, Texas.

0001-1541/78/9669-0072/$01.85

layer. The exact position of the flame can be calculated. It would be fine if the story ended here, but, unfortunately, for certain ranges of parameters there appear to be multiple solutions. For a certain range of oxygen ambient concentrations there may be three solutions for the same set of parameters. These solutions correspond to extinction, flame front in the boundary layer, or flame front in the ash layer. For a slightly higher range of ambient oxgyen concentrations, but not unreasonable, there are five solutions for the same parameters: extinction, two solutions with flame front at the core surface, a flame front in the ash layer, and a fifth with the flame front in the boundary layer. Most probably not all of these solutions are achievable (probably three are, the other two being unstable). These solutions lead to widely different gasification rates and conceivably would make it difficult to operate a reactor. It is apparent that a simple view of a burning carbon sphere must be abandoned, and it is also apparent that substantially more work needs to be done.

ASSUMPTIONS FOR THE MODEL

We will suppose that the devolatilized coal particle, that is char, is a homogeneous porous sphere consisting primarily of carbon and some ash. The particle is exposed in this study to an environment containing oxygen, carbon monoxide, carbon dioxide, water vapor, and inert, probably nitrogen The reactions which are assumed to take place are

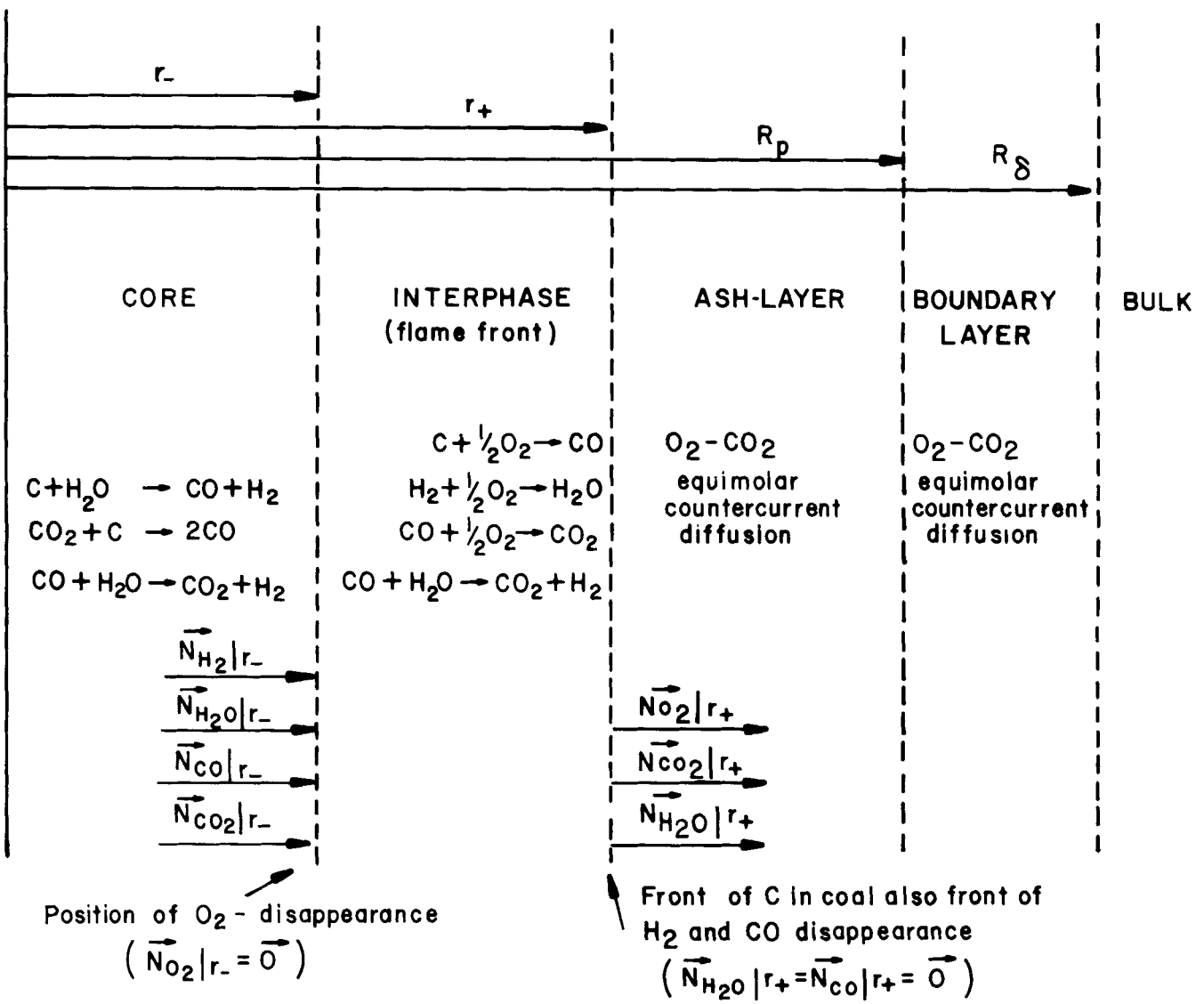

Fig. 1. Particle regions. Flame at core.

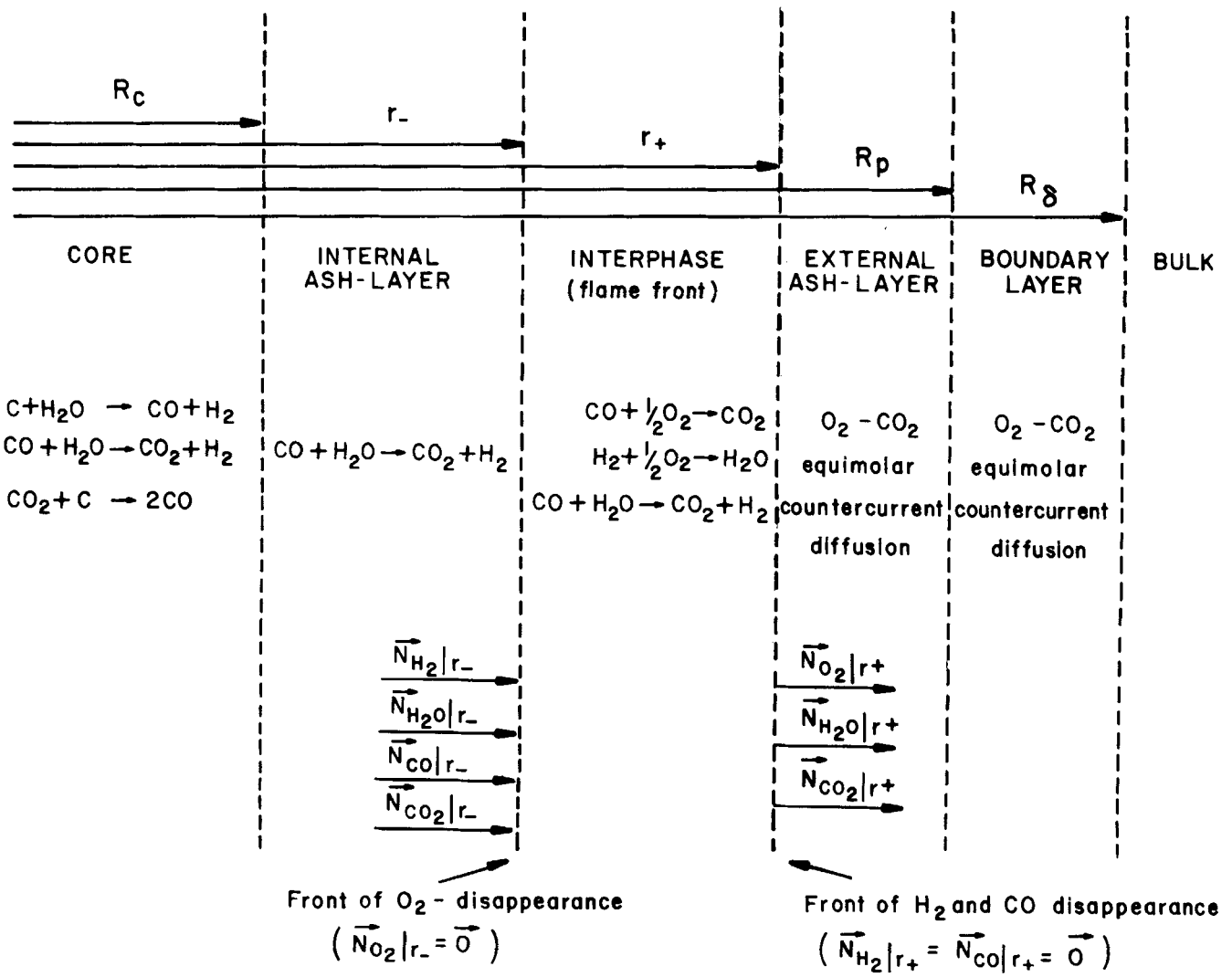

Fig. 2. Particle regions. Flame in ash layer.

R1: $\lambda C + O_2 \rightarrow 2(\lambda - 1)CO + (2 - \lambda)CO_2$
R2: $C + CO_2 \rightarrow 2CO$
R3: $C + H_2O \rightarrow CO + H_2$
R4: $CO + H_2O \rightarrow CO_2 + H_2$
R5: $H_2 + \frac{1}{2}O_2 \rightarrow H_2O$
R6: $CO + \frac{1}{2}O_2 \rightarrow CO_2$

The first three are heterogeneous, and the last three are homogeneous. The methanation reaction is ignored here since there is essentially no hydrogen present, as we shall demonstrate. Reactions R4 to R6 are known to be very fast and will be considered to be at equilibrium, and, since the equilibrium constants for reactions R5 and R6 are very large, the possibility of coexistence of hydrogen and oxygen or carbon monoxide and oxygen in appreciable amounts is unlikely. The direct combustion of carbon (reaction R1) produces a mixture of carbon monoxide and carbon dioxide in a proportion that is dependent on the surface temperature. Arthur (1951) has shown that at a high temperature, carbon monoxide is the main product. However, since we have assumed that carbon monoxide and oxygen cannot coexist, any carbon monoxide formed will be instantaneously burnt to carbon dioxide, and therefore R1 can be replaced by

$$\text{R1}'\text{: } C + O_2 \rightarrow CO_2$$

Reaction R1′ is relatively fast and will be assumed to cause a shrinking core model. By comparison, R2 and R3 are slow, and we will consider them to occur homogeneously within the core.

The assumption of noncoexistence of hydrogen and oxygen (or carbon monoxide and oxygen) is a particular application of the two-film theory developed by Burke and Schuman (1931) for carbon combustion and by several authors for liquid fuel droplet combustion. According to that theory, the gaseous fuel generated in the core (hydrogen and carbon monoxide in our case) reacts instantaneously with the incoming oxygen in a sharp front that is called the flame front and is located at a point where both fuel and oxygen fluxes are in the proper stoichiometric relation. Under conditions of low core temperature or high oxygen concentration in the bulk, the oxidant flux is always larger than the fuel flux, and oxygen can reach the external surface of the core. This excess of oxygen reacts there according to R1′ and produces the core shrinkage, and the flame front is at its maximum depth at the core surface. With a decreasing oxygen concentration in the particle environment, however, there may be no excess oxygen at the core surface, in which case the flame front will pull away from the core and be located at a point which must be determined. Depending on the position of the flame front, three different situations can develop in the particle, namely: flame front at the core surface, $R^* = R_c$; flame front in ash layer, $R_c < R^* < R_p$; and flame front in the boundary layer, $R_p < R^* < R_\delta$, where R^* represents the

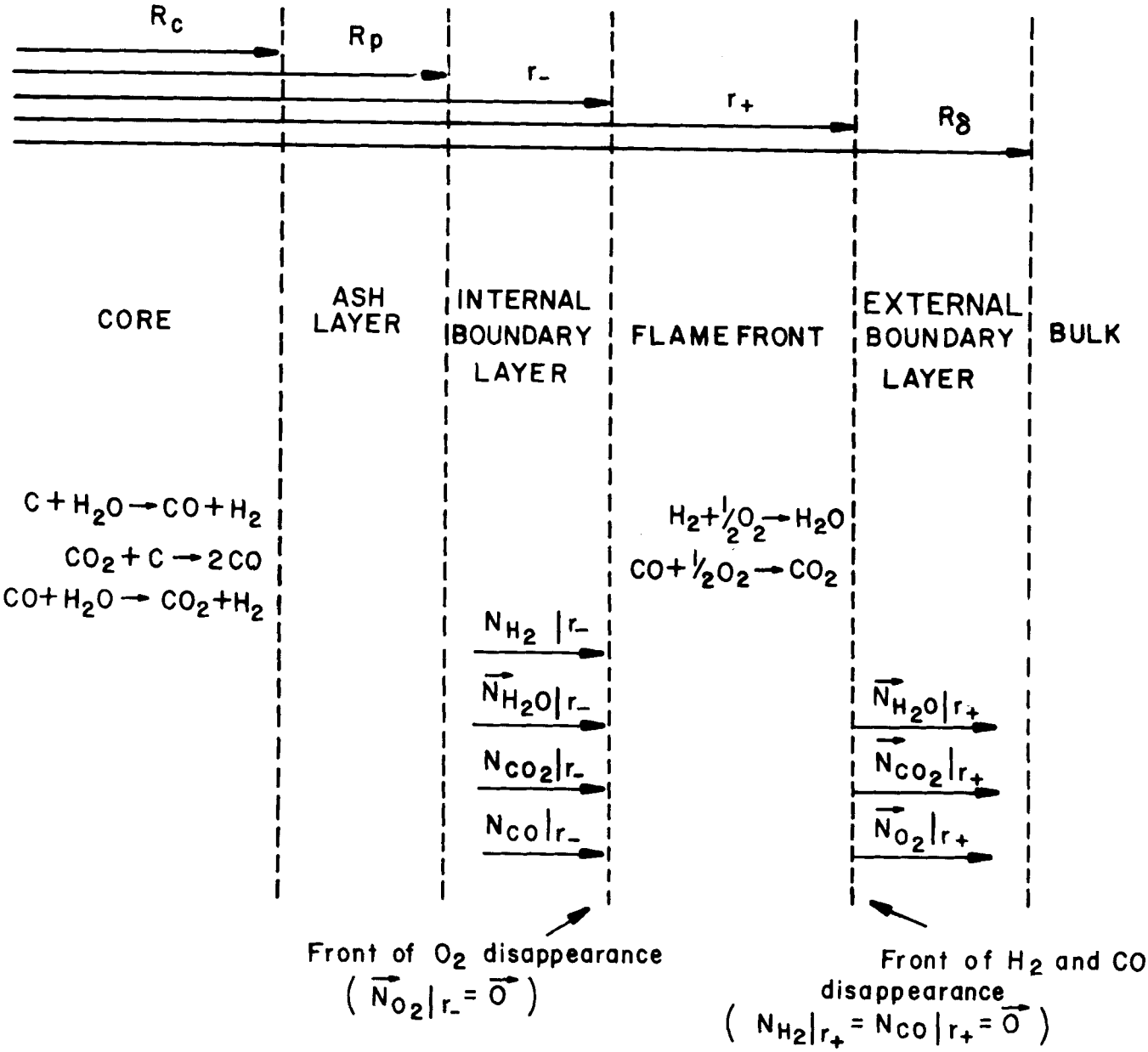

Fig. 3. Particle regions. Flame in boundary layer.

radius of the flame front. These three situations are pictured in Figures 1, 2, and 3, respectively. Observe that for each case the flame front divides the concentration and temperature fields into two distinct regions: an external region where the only process is a nonisothermal equimolar countercurrent diffusion of carbon dioxide and oxygen, and an internal region which always includes a lumped core but may comprise part of the ash layer or even all of it plus part of the boundary layer, where a multicomponent nonisothermal diffusion and reaction (water shift) process takes place. When the reacting surface and the core external surface do not coincide, the zone between them is difficult to describe. Two models are studied here: a homogeneous model in which one assumes that the diffusional processes are much faster than the reaction processes occurring in the core and thus the concentrations of all the species inside the reacting sphere are uniform and equal to their values at the flame, $x_{H_2} = x_{CO} = 0$ everywhere, and a heterogeneous model in which the Stephan-Maxwell equations are solved for $R_c < r < R^*$ with two additional assumptions. First, the binary diffusivity of hydrogen in any other species of the mixture, being much larger than for any other pair of species, is taken to be infinite $D_{H_2,j} = D_H = \infty$ for all j. Second, for any other pair of species, the binary diffusivity is a constant independent of the pair under consideration, $D_{ij} = D$, for all i, j not including hydrogen. The first assumption implies that $x_{H_2} = 0$ for all $r \leq R^*$, and because the water gas shift reaction is at equilibrium everywhere, $x_{CO} = 0$ for all $r \leq R^*$. The external region is not affected by any of the assumptions made to describe the internal zone.

KINETIC MECHANISM AND REACTION RATE EXPRESSIONS

The gasification of carbon by hydrogen, steam, or a mixture of the two has been studied by Blackwood (1962), Blackwood and McCarthy (1966), Blackwood and McGrory (1958), Wen and Huebler (1965), and some others. In this work, however, an empirical expression developed at the Institute of Gas Technology (IGT) by Johnson (1974) will be used and results compared with those obtained by using another em-

TABLE 1a. IGT KINETICS

R1: $C + H_2O \rightarrow CO + H_2$
R2: $C + 2H_2 \rightarrow CH_4$
R3: $2C + H_2 + H_2O \rightarrow CO + CH_4$

$$\frac{dX}{dt} = f_L k_T (1 - X)^{2/3} \exp(-\alpha X^2)$$

$$k_T = k_1 + k_2 + 2k_3$$

$$f_L = f_o \exp(8467/T_o)$$

$$k_1 = \frac{9\,380 \exp\left[-\frac{31\,705}{T}\right]\left(1 - \frac{p_{CO}p_{H_2}}{p_{H_2O} K_I^{eq}}\right)}{\left\{1 + \left(\exp\left[-22.216 + \frac{44\,787}{T}\right)\right]\left(\frac{1}{p_{H_2O}} + 16.35\frac{p_{H_2}}{p_{H_2O}} + 43.5\frac{p_{CO}}{p_{H_2O}}\right)\right\}^2} \text{ (min}^{-1}\text{)}$$

$$k_2 = \frac{16.5\, p^2_{H_2}\left[\exp\left(-\frac{33\,076}{T}\right)\right]\left(1 - \frac{p_{CH_4}}{p^2_{H_2} K_{II}^{eq}}\right)}{1 + p_{H_2}\left[\exp\left(-10.4520 + \frac{19\,976}{T}\right)\right]} \text{ (min}^{-1}\text{)}$$

$$k_3 = \frac{p^{1/2}_{H_2} p_{H_2O}\left[\exp\left(11.8794 - \frac{44\,544}{T}\right)\right]\left(1 - \frac{p_{CO}p_{CH_4}}{p_{H_2}p_{H_2O} K_{III}^{eq}}\right)}{\left\{1 + \left[\exp\left(-6.6696 + \frac{15\,198}{T}\right)\right]\left(p^{1/2}_{H_2} + 0.85\, p_{CO} + 18.6\frac{p_{CH_4}}{p_{H_2}}\right)\right\}^2} \text{ (min}^{-1}\text{)}$$

$$\alpha = 0.969 + \frac{0.103\, p^{1/2}_{H_2} p_{H_2O}}{1 + 0.137\, p^{1/2}_{H_2} p_{H_2O}}$$

where:
K_i^{eq} = equilibrium constant of reaction i, carbon as graphite
T = reaction temperature, °R
p_i = partial pressure of i^{th} component, atm
T_o = maximum temperature to which char has been exposed previous to gasification if °R (If $T_o < T$, $T_o = T$)
f_o = relative reactivity factor characteristic for each coal

TABLE 1b. GIBSON-EUKER

Rxm: $C + H_2O \rightarrow CO + H_2$

$$\text{Rate} = k\left(p_{H_2O} - \frac{p_{CO}\, p_{H_2}}{k^{eq}}\right)\left(\frac{\text{moles of } C \text{ converted}}{\text{moles of } C \text{ present} \times \text{s}}\right)$$

$$k = k_o e^{-E/RT}$$

	k_o $\left(\frac{\text{moles of } C \text{ converted}}{\text{moles of } C \text{ reacted} \times \text{s}}\right)$	E $\left(\frac{\text{kcal}}{\text{mole}}\right)$
Illinois Coal (low reactivity)	550	42
Wyoming Coal (high reactivity)	360	35

Notes
1. In the combustion zone, $p_{H_2} = p_{CO} = 0$
2. Rate of reaction per unit core surface area

$$Q_{H_2O} = \frac{\rho_{FC}(1 - X)}{M_c}\frac{R_c}{3} k\, p_{H_2O}$$

pirical expression presented by Gibson and Euker (1975). For the IGT kinetic scheme, three basic reactions are assumed to occur:

Reaction I: $C + H_2O \rightarrow CO + H_2$

Reaction II: $C + 2H_2 \rightarrow CH_4$

Reaction III: $2C + H_2O + H_2 \rightarrow CH_4 + CO$

The water-gas shift reaction is assumed to be at equilibrium. Reaction III is not stoichiometrically independent of the first two but is used for experimental data correlation purposes and was suggested by Blackwood and McGrory (1958) to justify the finding that the methane concentration can be larger than the equilibrium value. If we define a conversion referred to the fixed carbon in a particle by

$$X = \frac{\text{mass of carbon gasified}}{\text{mass of fixed carbon in feed}}$$

where the fixed carbon is the carbon in the coal particle less the carbon associated with the volatile components, the rate of change of the conversion can be correlated to give

$$\frac{dX}{dt} = k_T \beta$$

where

$$k_T = k_1 + k_2 + 2k_3$$

$$\beta = f_L(1 - X)^{2/3} \exp(-\alpha X^2)$$

and k_1, k_2, k_3 are the individual rate constants for each of the above reactions and are shown in Table 1 as is the relative reactivity of the coal which depends on a number of factors. If we call Q_{H_2O} the rate of carbon conversion in moles of carbon gasified per unit time per unit particle volume, since the particle is considered to be of constant radius, we can write

$$Q_{H_2O} = \frac{\rho_{CF}}{M_c}\frac{dX}{dt} = \frac{\rho_{CF}}{M_c}\beta k_T$$

Since the gasification of the carbon occurs by steam or by carbon dioxide, and since both species are present in the reaction mixture, the net rate of carbon gasification given by Q_{H_2O} includes both mechanisms in the sense that the water gas shift equilibrium is affected by the presence of carbon dioxide. In the empirical correlations, no mention is made of carbon dioxide gasifica-

tion other than that the water-gas shift reaction is at equilibrium. Another type of kinetic mechanism considered here is that of Gibson-Euker. Two types of coals were investigated: Illinois or low reactivity and Wyoming or high reactivity coal. The steam-carbon reaction was found to be first order in both carbon concentration and steam partial pressure and reversible, while temperature dependence was found to follow the typical Arrhenius form with a characteristic frequency factor and activation energy for each of the coals investigated. The water-gas shift reaction is assumed to be in equilibrium. The temperature range investigated is more limited than in the work at IGT, that is, below 1225K for the steam-carbon gasification and below 1175K for the methane decomposition. The main advantage of this kinetic expression is the simple form it reduces to for the combustion zone of a Lurgi gasifier (hydrogen and carbon monoxide concentrations are negligible and the steam gasification becomes first order in p_{H_2O} and irreversible). For the carbon combustion reaction, $C + \frac{1}{2}O_2 \rightarrow CO$, the expression to be used will be that given by Field et al. (1967):

$$R_t = 726\, P \exp\left(-\frac{17\,850}{T_c}\right) x_{O_2}\left(\frac{\text{g mole}}{\text{cm}^2\,\text{s}}\right)$$

It will be assumed that changes in core conversion due to the steam gasification do not affect the carbon combustion reaction rate.

MASS CONSERVATION EQUATIONS

Flame Front at Core Surface

The situation is pictured in Figure 1. The reactions occurring within the core are the steam gasification (R3), the gasification with carbon dioxide (R2), and the water-gas shift (R4). Oxygen reaching the core surface will be consumed by reaction with hydrogen and carbon monoxide produced in the core and by reaction with solid carbon according to R_1'. A balance across the flame front leads to

$$\tfrac{1}{2}[N_{H_2}|_{R_c^-} + N_{CO}|_{R_c^-}] + R_1 = -N_{O_2}|_{R_c^+}$$

In the core we have

$$N_{H_2}|_{R_c^-} + N_{CO}|_{R_c^-} = 2\frac{R_c}{3}(Q_{H_2O})$$

and the first equation becomes

$$-N_{O_2}|_{R_c^+} = R_1 + \frac{R_c}{3}(Q_{H_2O}) \tag{1}$$

As neither hydrogen nor carbon monoxide cross the reacting surface, $N_{H_2} = 0 = N_{CO}$ for all $r \geq R^*$. Two important conclusions can now be derived: the net process from the viewpoint outside the core will be a net reaction $C + O_2 \rightarrow CO_2$ completed at the reacting surface, and no net flux of water occurs and therefore $x_{H_2O} = x_{H_2O,B}$ everywhere. Consequently, outside the core a countercurrent equimolar diffusion of oxygen and carbon dioxide takes place, and the oxygen concentration distribution can be found by solving the conservation equations for oxygen

$$\frac{1}{r^2}\frac{d}{dr}\left[r^2 cD_e \frac{dx_{O_2}}{dr}\right] = 0; \quad R_c = R^* < r < R_p \tag{2}$$

$$\frac{1}{r^2}\frac{d}{dr}\left[r^2 cD \frac{dx_{O_2}}{dr}\right] = 0, \quad R_p < r < R_\delta \tag{3}$$

together with the continuity conditions at $r = R_p$ for the concentrations and fluxes

$$cD_e \frac{dx_{O_2}}{dr}\bigg|_{R_p^-} = cD \frac{dx_{O_2}}{dr}\bigg|_{R_p^+} \tag{4}$$

$$x_{O_2}|_{R_p^-} = x_{O_2}|_{R_p^+} \tag{5}$$

and the known condition at the external edge of the boundary layer

$$x_{O_2} = x_{O_2,B}, \quad r = R_\delta \tag{6}$$

and the flux at the core surface given by Equation (1) which can also be written as

$$cD_e \frac{dx_{O_2}}{dr} = R_1 + \frac{R_c}{3}(Q_{H_2O}) = Q, \quad r = R_c \tag{7}$$

The resulting oxygen mole fraction profile is presented

Table 2. Oxygen Concentration Profile

Flame front at core surface

$$x_{O_2} = \begin{cases} 0, & r < R_c \\ x_{O,2B} - \dfrac{QR_c^2}{cD}\left[\left(\dfrac{1}{R_p} - \dfrac{1}{R_\delta}\right) + \dfrac{1}{\epsilon^2}\left(\dfrac{1}{r} - \dfrac{1}{R_p}\right)\right], & R_c \leq r \leq R_p \\ x_{O_2,B} - \dfrac{QR_c^2}{cD}\left(\dfrac{1}{r} - \dfrac{1}{R_\delta}\right), & R_p \leq r \leq R_\delta \end{cases}$$

Flame front in ash layer

$$x_{O_2} = \begin{cases} 0, & r \leq R^* \\ x_{O_2,B} - \dfrac{Q_{H_2O}R_c^2}{cD}\left[\left(\dfrac{1}{R_p} - \dfrac{1}{R_\delta}\right) + \dfrac{1}{\epsilon^2}\left(\dfrac{1}{r} - \dfrac{1}{R_p}\right)\right], & R^* \leq r \leq R_p \\ x_{O_2,B} - \dfrac{Q_{H_2O}R_c^2}{cD}\left(\dfrac{1}{r} - \dfrac{1}{R_\delta}\right), & R_p \leq r \leq R_\delta \end{cases}$$

Flame front in boundary layer

$$x_{O_2} = \begin{cases} 0, & r \leq R^* \\ x_{O_2,B} - \dfrac{Q_{H_2O}R_c^2}{cD}\left(\dfrac{1}{r} - \dfrac{1}{R_\delta}\right), & R^* \leq r \leq R_\delta \end{cases}$$

in Table 2, and in its derivation it has been assumed that

$$D_e = \epsilon^2 D$$

From those results, x_{O_2} at $r = R_c$ can be computed, and since

$$R_1 = K_1 x_{O_2}|_{r=R_c}$$

the total rate of C consumption per unit area of core surface can be written as

$$Q = \frac{K_1 x_{O_2,B} + Q_{H_2O}(T_c, x_{H_2O,B})}{1 + \frac{K_1 R_c^2}{cD}\left[\left(\frac{1}{R_p} - \frac{1}{R_\delta}\right) + \frac{1}{\epsilon^2}\left(\frac{1}{R_c} - \frac{1}{R_p}\right)\right]}$$

Flame Front Outside Core

If the temperature of the core becomes too large or the concentration of oxygen in the bulk too low, the flame front will separate from the core surface and move to the ash layer or to the gas film around the particle. The total rate of C consumption will now be given by Q_{H_2O} because $x_{O_2} = 0$ at core surface. If the flame front is in the ash layer, the oxygen conservation Equations (2) and (3), the continuity conditions at $r = R_p$, (4) and (5), and the boundary condition at $r = R_\delta$ (6) still hold, but the oxygen flux at the reacting surface (7) is now given by

$$\epsilon^2 cD \frac{dx_{O_2}}{dr} = \left(\frac{R_c}{R^*}\right)^2 Q_{H_2O}, \quad r = R^*$$

If, however, the flame front is in the gas film, we can write the following system of equations:

$$\frac{1}{r^2}\frac{d}{dr}\left(r^2 cD \frac{dx_{O_2}}{dr}\right) = 0, \quad R^* < r < R_p$$

$$cD \frac{dx_{O_2}}{dr} = \left(\frac{R_c}{R^*}\right)^2 Q_{H_2O}, \quad r = R^*$$

$$x_{O_2} = x_{O_2,B}, \quad r = R_p$$

The physical situation is summarized in Figures 2 and 3, respectively. In either case, the oxygen mole fraction profile can be obtained, and it is presented in Table 2.

An extra condition, namely, the fact that the oxygen concentration becomes zero at the flame front, allows us to compute the radius of that reacting surface:

$$R^* = \frac{R_p}{\frac{cD\epsilon^2 x_{O_2,B} R_p}{Q_{H_2O} R_c^2} + 1 - \epsilon^2 + \frac{R_p}{R_\delta}\epsilon^2}, \quad \text{for } R_c < R^* < R_p \quad (8)$$

and

$$R^* = \frac{1}{\frac{cDx_{O_2,B}}{Q_{H_2O}R_c^2} + \frac{1}{R_\delta}}, \quad R^* \geq R_p \quad (9)$$

CONSERVATION OF ENERGY EQUATION

The energy conservation equation

$$\nabla \cdot (q + \Sigma N_i h_i) = 0$$

can be expanded to give

$$-\nabla \cdot (K \nabla T) + \Sigma h_i \nabla \cdot N_i + \Sigma N_i \cdot \nabla h_i = 0$$

with

$$\nabla h_i = C_{pi} \nabla T$$

Because of the relatively high thermal conductivity of the core, it is assumed to be at uniform temperature T_c.

Flame Front at Core Surface

Taking into account mass conservation and calling

$$\Delta C_{pI} = C_{pO_2} - C_{pCO_3}$$

the energy equations to be solved are

$$\frac{1}{r^2}\frac{d}{dr}\left(K_e r^2 \frac{dT}{dr}\right) + \Delta C_{pI} Q \frac{R_c^2}{r^2}\frac{dT}{dr} = 0, \quad R_c = R^* < r < R_p \quad (10)$$

$$\frac{1}{r^2}\frac{d}{dr}\left(Kr^2 \frac{dT}{dr}\right) + \Delta C_{pI} Q \frac{R_c^2}{r^2}\frac{dT}{dr} = 0, \quad R_p < r < R_\delta \quad (11)$$

Since the net process at the core surface is given by the reaction $C + O_2 \rightarrow CO_2$, the boundary condition there is

$$K_e \frac{dT}{dr} = Q\Delta H_c, \quad r = R_c$$

If we now incorporate the continuity conditions at the ash-gas interface

$$K_e \frac{dT}{dr}\bigg|_{R_p^-} = K \frac{dT}{dr}\bigg|_{R_p^+}, \quad r = R_p \quad (12)$$

$$T|_{R_p^-} = T|_{R_p^+}, \quad r = R_p \quad (13)$$

together with the known bulk temperature at the external edge of the film

$$T = T_B, \quad r = R_\delta \quad (14)$$

the system of equations can be solved and the temperature profile, shown in Table 3, obtained.

Flame Front Outside Core Surface

Both the homogeneous and the inhomogeneous models with the assumptions of $x_{H_2} \cong 0$ everywhere and water-gas shift reaction in equilibrium reduce the complex situation that arises when the flame front moves outside the core surface to a lumped core where the net reaction

$$C + 2H_2O \rightarrow CO_2 + 2H_2$$

takes place at a net rate Q_{H_2O} and to an intermediate shell located between the core and the reacting surface where nonchemically interacting species are diffusing. If the flame front is in the ash layer, the energy conservation equation for such a shell reduces to

$$\frac{1}{r^2}\frac{d}{dr}\left(r^2 K_e \frac{dT}{dr}\right) + \Delta C_{pII} Q_{H_2O}\left(\frac{R_c}{r}\right)^2 \frac{dT}{dr} = 0, \quad R_c < r < R^* \quad (15)$$

where

$$\Delta C_{pII} = C_{pCO_2} + 2C_{pH_2} - 2C_{pH_2O}$$

Outside the core, Equations (10) and (11), the continuity conditions at $r = R_p$, (12) and (13), and the boundary condition at $r = R_\delta$, (14), still hold. The boundary condition at the core surface will now be

$$K_e \frac{dT}{dr} = \Delta H_I Q_{H_2O}, \quad r = R_c$$

with ΔH_I the change of enthalpy for the reaction $C + 2H_2O \rightarrow CO_2 + 2H_2$. At the flame we impose temperature continuity

$$T|_{R^*-} = T|_{R^*+}, \quad r = R^*$$

and continuity of fluxes

$$-K_e \frac{dT}{dr}\bigg|_{R^*-} + \Sigma N_i h_i|_{R^*-}$$

TABLE 3. TEMPERATURE PROFILES

'lame front at core surface

$$= \begin{cases} T_c, r \leq R_c \\ T_B - \dfrac{\Delta H_c}{\Delta C_{pI}} \left\{ \exp\left[\alpha_{eI} \left(\dfrac{1}{r} - \dfrac{1}{R_c} \right) \right] - \exp\left[\alpha_{eI} \left(\dfrac{1}{R_p} - \dfrac{1}{R_c} \right) \right] \exp\left[\alpha_I \left(\dfrac{1}{R_\delta} - \dfrac{1}{R_p} \right) \right] \right\} & , R_c \leq r \leq R_p \\ T_B - \dfrac{\Delta H_c}{\Delta C_{pI}} \exp\left[\alpha_{eI} \left(\dfrac{1}{R_p} - \dfrac{1}{R_c} \right) \right] \left\{ \exp\left[\alpha_I \left(\dfrac{1}{r} - \dfrac{1}{R_p} \right) - \exp\left[\alpha_I \left(\dfrac{1}{R_\delta} - \dfrac{1}{R_p} \right) \right] \right] \right\} & , R_p \leq r \leq R_\delta \end{cases}$$

'lame front in ash layer

$$= \begin{cases} T_c, r \leq R_c \\ T_B + \left\{ \dfrac{\Delta H_I}{\Delta C_{pII}} \exp\left[\alpha_{eII} \left(\dfrac{1}{R^*} - \dfrac{1}{R_c} \right) \right] + \dfrac{2\,\Delta H_w}{\Delta C_{pI}} \right\} \cdot \left\{ \exp\left[\alpha_{eI} \left(\dfrac{1}{R_p} - \dfrac{1}{R^*} \right) \right] \cdot \exp\left[\alpha_I \left(\dfrac{1}{R_p} - \dfrac{1}{R_\delta} \right) \right] - 1 \right\} \\ \quad + \dfrac{\Delta H_I}{\Delta C_{pII}} \left\{ \exp\left[\alpha_{eII} \left(\dfrac{1}{R^*} - \dfrac{1}{R_c} \right) \right] - \exp\left[\alpha_{eII} \left(\dfrac{1}{r} - \dfrac{1}{R_c} \right) \right] \right\} & , R_c \leq r \leq R_c \\ T_B + \left\{ \dfrac{\Delta H_I}{\Delta C_{pI}} \exp\left[\alpha_{eII} \left(\dfrac{1}{R^*} - \dfrac{1}{R_c} \right) \right] + \dfrac{2\,\Delta H_w}{\Delta C_{pI}} \right\} \cdot \left\{ \exp\left[\alpha_{eI} \left(\dfrac{1}{R_p} - \dfrac{1}{R^*} \right) \right] \cdot \exp\left[\alpha_I \left(\dfrac{1}{R_\delta} - \dfrac{1}{R_p} \right) \right] \right. \\ \quad \left. - \exp\left[\alpha_{eI} \left(\dfrac{1}{r} - \dfrac{1}{R^*} \right) \right] \right\} & , R^* \leq r \leq R_p \\ T_B + \left\{ \dfrac{\Delta H_I}{\Delta C_{pI}} \exp\left[\alpha_{eII} \left(\dfrac{1}{R^*} - \dfrac{1}{R_c} \right) \right] + 2 \dfrac{\Delta H_w}{\Delta C_{pI}} \right\} \exp\left[\alpha_{eI} \left(\dfrac{1}{R_p} - \dfrac{1}{R^*} \right) \right] \cdot \left\{ \exp\left[\alpha_I \left(\dfrac{1}{R_\delta} - \dfrac{1}{R_p} \right) \right] \right. \\ \quad \left. - \exp\left[\alpha_I \left(\dfrac{1}{r} - \dfrac{1}{R_p} \right) \right] \right\} & , R_p \leq r \leq R_\delta \end{cases}$$

'lame front in boundary layer

$$= \begin{cases} T_c, r \leq R_c \\ T_B + \dfrac{\Delta H_I}{\Delta C_{pII}} \left\{ \exp\left[\alpha_{eII} \left(\dfrac{1}{R_p} - \dfrac{1}{R_c} \right) \right] \exp\left[\alpha_{II} \left(\dfrac{1}{R^*} - \dfrac{1}{R_p} \right) \right] - \exp\left[\alpha_{eII} \left(\dfrac{1}{r} - \dfrac{1}{R_c} \right) \right] \right\} + \left\} \dfrac{\Delta H_I}{\Delta C_{pI}} \exp\left[\right. \right. \\ \alpha_{eII} \left(\dfrac{1}{R_p} - \dfrac{1}{R_c} \right) \left. \right] \exp\left[\alpha_{II} \left(\dfrac{1}{R^*} - \dfrac{1}{R_p} \right) \right] + \dfrac{2\Delta H_w}{\Delta C_{pI}} \left. \right\} \left\{ \exp\left[\alpha_I \left(\dfrac{1}{R_\delta} - \dfrac{1}{R^*} \right) \right] - 1 \right\} & , R_c \leq r \leq R_p \\ T_B + \dfrac{\Delta H_I}{\Delta C_{pII}} \exp\left[\alpha_{eII} \left(\dfrac{1}{R_p} - \dfrac{1}{R_c} \right) \right] \left\{ \exp\left[\alpha_{II} \left(\dfrac{1}{R^*} - \dfrac{1}{R_p} \right) \right] - \exp\left[\alpha_{II} \left(\dfrac{1}{r} - \dfrac{1}{R_p} \right) \right] \right\} + \left\{ \dfrac{\Delta H_I}{\Delta C_{pI}} \exp\left[\right. \right. \\ \alpha_{eII} \left(\dfrac{1}{R_p} - \dfrac{1}{R_c} \right) \left. \right] \exp\left[\alpha_{II} \left(\dfrac{1}{R^*} - \dfrac{1}{R_p} \right) \right] + \dfrac{2\Delta H_w}{\Delta C_{pI}} \left. \right\} \left\{ \exp\left[\alpha_I \left(\dfrac{1}{R_\delta} - \dfrac{1}{R^*} \right) \right] - 1 \right\} & , R_p \leq r \leq R^* \\ T_B + \left\{ \dfrac{\Delta H_I}{\Delta C_{pI}} \exp\left[\alpha_{eII} \left(\dfrac{1}{R_p} - \dfrac{1}{R_c} \right) \right] \exp\left[\alpha_{II} \left(\dfrac{1}{R^*} - \dfrac{1}{R_p} \right) \right] + \dfrac{2\Delta H_w}{\Delta C_{pI}} \right\} \cdot \left\{ \exp\left[\alpha_I \left(\dfrac{1}{R_\delta} - \dfrac{1}{R^*} \right) \right] \right. \\ \quad \left. - \exp\left[\alpha_I \left(\dfrac{1}{r} - \dfrac{1}{R^*} \right) \right] \right\} & , R^* \leq r \leq R_\delta \end{cases}$$

$$= -K_e \frac{dT}{dr}\bigg|_{R^*+} + \Sigma N_i h_i|_{R^*+}$$

If we introduce the results from mass conservation, the last expression becomes

$$-K_e \frac{dT}{dr}\bigg|_{R^*-} = -K_e \frac{dT}{dr}\bigg|_{R^*+} + 2Q_{H_2O}\Delta H_w \left(\frac{R_c}{R^*} \right)^2$$

where ΔH_w is the enthalpy change for the reaction $H_2 + \frac{1}{2}O_2 \rightarrow H_2O$. If we solve the system, the temperature profile can be obtained and is presented in Table 3. If the flame front is in the gas film, Equation (15) is valid for the whole ash layer, and an equivalent equation can be written for the shell that extends from $r = R_p$ to $r = R^*$. For the outer region, Equation (11) holds. In a similar fashion as before, the boundary conditions can be written. The temperature profile obtained is again presented in Table 3.

Of special importance to us is to relate core temperatures to the bulk temperature. This is a straightforward relation starting from the profiles given in Table 3. Such relations are shown in Table 4. Simple preliminary computations show that differences in specific heats can be neglected with little error. Values of the bulk temperature as a function of the core temperature T_c and either flame position (R^*) or oxygen ambient concentration are also given in Table 4 with this assumption.

TABLE 4. RELATION BETWEEN T_B AND T_c

Flame front at core surface

$$T_B = T_c + \frac{\Delta H_c}{\Delta C_{pI}} \left\{ 1 - \exp\left[\alpha_I \left(\frac{1}{R_\delta} - \frac{1}{R_p} \right) \right] \exp\left[\alpha_{eI} \left(\frac{1}{R_p} - \frac{1}{R_c} \right) \right] \right\}$$

Flame front in ash layer

$$T_B = T_c + \left\{ \frac{\Delta H_I}{\Delta C_{pI}} \exp\left[\alpha_{eII} \left(\frac{1}{R^*} - \frac{1}{R_c} \right) \right] + \frac{2\Delta H_w}{\Delta C_{pI}} \right\} \left\{ 1 - \exp\left[\alpha_{eI} \left(\frac{1}{R_p} - \frac{1}{R^*} \right) \right] \cdot \exp\left[\alpha_I \left(\frac{1}{R_\delta} - \frac{1}{R_p} \right) \right] \right\} + \frac{\Delta H_I}{\Delta C_{pII}} \left\{ 1 - \exp\left[\alpha_{eII} \left(\frac{1}{R^*} - \frac{1}{R_c} \right) \right] \right\}$$

Flame front in boundary layer

$$T_B = T_c + \left\{ \frac{\Delta H_I}{\Delta C_{pI}} \exp\left[\alpha_{eII} \left(\frac{1}{R_p} - \frac{1}{R_c} \right) \right] \exp\left[\alpha_{II} \left(\frac{1}{R^*} - \frac{1}{R_p} \right) \right] + \frac{2\Delta H_w}{\Delta C_{pI}} \right\} \cdot \left\{ 1 - \exp\left[\alpha_I \left(\frac{1}{R} - \frac{1}{R^*} \right) \right] \right\} + \frac{\Delta H_I}{\Delta C_{pII}} \left\{ 1 - \exp\left[\alpha_{eII} \left(\frac{1}{R_p} - \frac{1}{R_c} \right) \right] \cdot \exp\left[\alpha_{II} \left(\frac{1}{R^*} - \frac{1}{R_p} \right) \right] \right\}$$

Relation between T_B and T_c when differences in C_p's neglected

I. In terms of R^*

$$T_B = \begin{cases} T_c + \Delta H_c Q R_c^2 \left[\frac{1}{K} \left(\frac{1}{R_p} - \frac{1}{R_\delta} \right) + \frac{1}{K_e} \left(\frac{1}{R_c} - \frac{1}{R_p} \right) \right], & R^* = R_c \\ T_c + Q R_c^2 \left\{ \Delta H_c \left[\frac{1}{K} \left(\frac{1}{R_p} - \frac{1}{R_\delta} \right) + \frac{1}{K_e} \left(\frac{1}{R^*} - \frac{1}{R_p} \right) \right] + \Delta H_I \frac{1}{K_e} \left(\frac{1}{R_c} - \frac{1}{R^*} \right) \right\}, & R_c \leq R^* \leq R_p \\ T_c + Q R_c^2 \left\{ \Delta H_c \frac{1}{K} \left(\frac{1}{R^*} - \frac{1}{R_\delta} \right) + \Delta H_I \left[\frac{1}{K} \left(\frac{1}{R_p} - \frac{1}{R^*} \right) + \frac{1}{K_e} \left(\frac{1}{R_c} - \frac{1}{R_p} \right) \right] \right\}, & R_p \leq R^* \leq R_\delta \end{cases}$$

II. In terms of $x_{O_2,B}$

$$T_B = \begin{cases} T_c + \Delta H_c Q R_c^2 \left[\frac{1}{K} \left(\frac{1}{R_p} - \frac{1}{R_\delta} \right) + \frac{1}{K_e} \left(\frac{1}{R_c} - \frac{1}{R_p} \right) \right], & R^* = R_c \\ T_c + Q R_c^2 \left\{ \Delta H_c \left(\frac{1}{R_p} - \frac{1}{R_\delta} \right) \left(\frac{1}{K} - \frac{\epsilon^2}{K_e} \right) + \frac{\Delta H_I}{K_e} \left[\left(\frac{1}{R_c} - \frac{1}{R_p} \right) + \epsilon^2 \left(\frac{1}{R_p} - \frac{1}{R_\delta} \right) \right] \right\} + \frac{c D x_{O_2,B} \epsilon^2}{K_e} (\Delta H_c - \Delta H_I), & R_c \leq R^* \leq R_p \\ T_c + Q R_c^2 \Delta H_I \left[\frac{1}{K} \left(\frac{1}{R_p} - \frac{1}{R_\delta} \right) + \frac{1}{K_e} \left(\frac{1}{R_c} - \frac{1}{R_p} \right) \right] + \frac{c D x_{O_2,B}}{K} (\Delta H_c - \Delta H_I), & R_p \leq R^* \leq R_\delta \end{cases}$$

The heterogeneous model accounts for the diffusional resistance between the core surface and flame front. Only the value of x_{H_2O} at the core surface will be affected. Notice, however, that the flame front separation from the core occurs at high values for T_c, and under those conditions the kinetic expression derived by Johnson becomes essentially of zero order with respect to x_{H_2O}. Therefore, if such kinetics are used, differences between models should be minor. This is not true for Gibson-Euker's kinetic model which shows a first-order dependence on x_{H_2O} for all temperatures.

If two different binary diffusivities are used, D_H for hydrogen in any other species and D for any pair that does not include hydrogen, the Stephan-Maxwell relations

$$\nabla x_i = \sum_{j=1}^{n} \frac{1}{c D_{ij}} (x_i N_j - x_j N_i) \qquad (16)$$

become

$$\nabla x_i = \frac{1}{cD} \left[x_i \sum_j N_j + x_i N_{H_2} \left(\frac{D}{D_H} - 1 \right) - x_{H_2} N_i \left(\frac{D}{D_H} - 1 \right) - N_i \right] \qquad (17)$$

for all species except hydrogen and

$$\nabla x_{H_2} = \frac{1}{c D_H} \left[x_{H_2} \sum_j N_j - N_{H_2} \right] \qquad (18)$$

for hydrogen. In the ash layer with the assumption of $D_{e,ij} = \epsilon^2 D_{ij}$, the right-hand sides of Equations (16) and (18) should be multiplied by a factor of $1/\epsilon^2$. If in addition we assume D_H to be very large, Equation (18) becomes

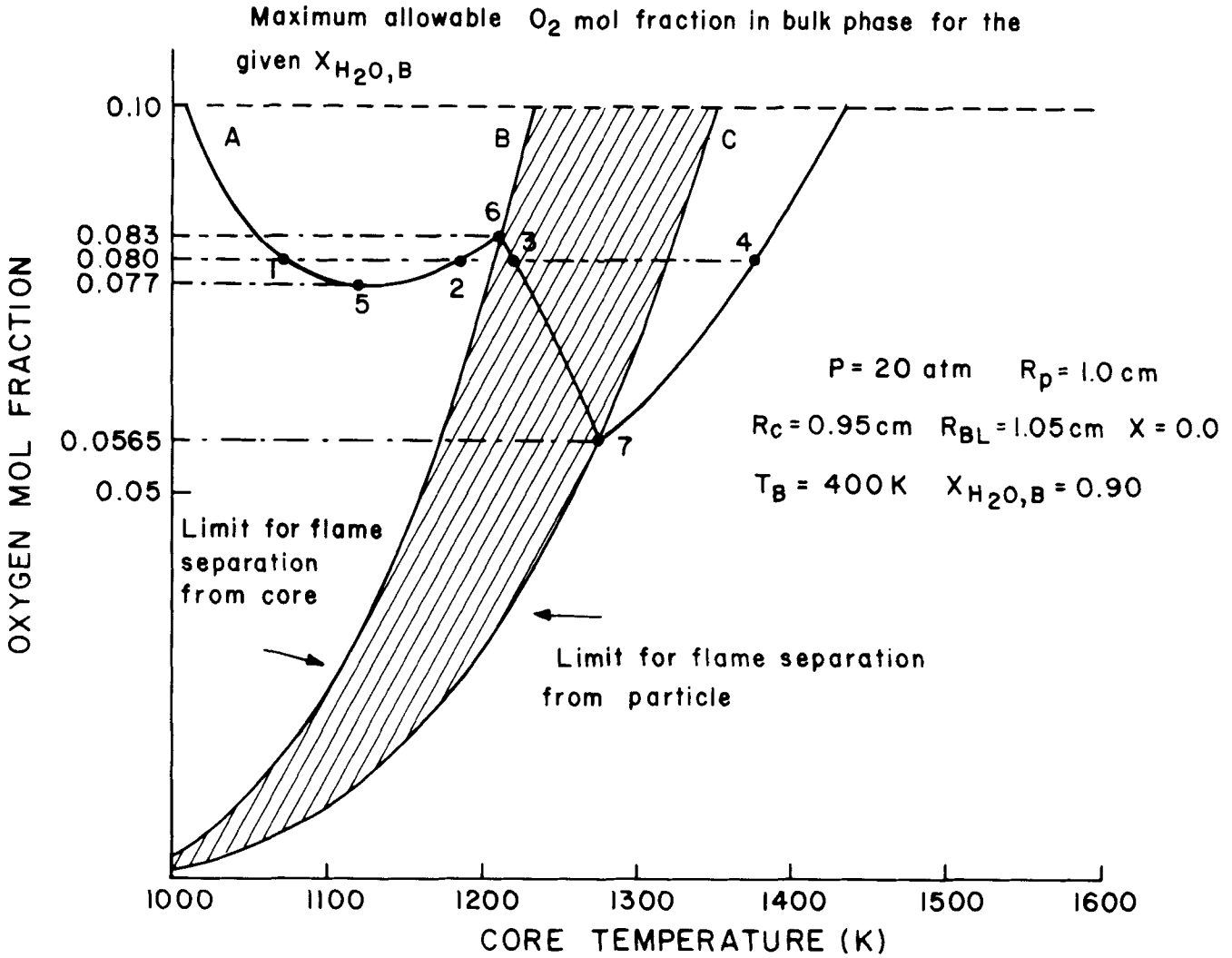

Fig. 4. Example of method of analysis [Johnson kinetic expression, (f_o = 1.0)].

$$\nabla x_{H_2} = 0$$

Knowing that $x_{H_2} = 0$ in the flame and using the postulate of equilibrium of the water-gas shift reaction, we obtain $x_{H_2} = x_{CO} = 0$ for all $r \leq R^*$, and Equation (17) reduces to

$$\nabla x_i = \frac{1}{cD}\left[x_i \Sigma N_j - x_i N_{H_2} - N_i\right] \tag{19}$$

We have already seen that under these conditions the net reaction at the core will be

$$C + 2H_2O \rightarrow CO_2 + 2H_2$$

occurring at a rate Q_{H_2O}. From the stoichiometry we can write

$$N_{CO_2}|_{R_c} = -\tfrac{1}{2}N_{H_2O}|_{R_c} = \tfrac{1}{2}N_{H_2}|_{R_c} = Q_{H_2O}$$

Since no reaction occurs in the zone between core and flame front, we can write

$$N_i = a_i N_{H_2O} \tag{20}$$

where

$$a_i = \frac{\alpha_i}{\alpha_{H_2O}}$$

and α_i is the stoichiometric coefficient of i^{th} species in the core net reaction ($\alpha_i = 0$ for an inert such as N_2). Therefore

$$\Sigma N_j = N_{H_2O}\Sigma a_i = -\tfrac{1}{2}N_{H_2O} \tag{21}$$

Substituting (20) and (21) back into (19), and because $a_{H_2} = -1$, we get

$$\nabla x_i = \frac{1}{cD}\left(\frac{x_i}{2} - a_i\right) N_{H_2O} \tag{22}$$

If we are working in the ash layer, (22) should be replaced by

$$\nabla x_i = \frac{1}{\epsilon^2 cD}\left(\frac{x_i}{2} - a_i\right) N_{H_2O} \tag{23}$$

With water as a key component, Equations (22) or (23) give

$$\frac{\nabla x_i}{\frac{x_i}{2} - a_i} = \frac{\nabla x_{H_2O}}{\frac{x_{H_2O}}{2} - a_{H_2O}}$$

which on integration yields

$$x_i = \frac{x_i^* - 2a_i}{x^*_{H_2O} - 2a_{H_2O}}\left(x_{H_2O} - 2a_{H_2O}\right) + 2a_i$$

where the asterisk indicates known mole fractions at some point (the flame front in this case). As there is no net flow of nitrogen or water in the outer shell, $x_{N_2}^* = x_{N_2,B}$ and $x^*_{H_2O} = x_{H_2O,B}$. Consequently

$$x^*_{CO_2} = 1 - x^*_{H_2O} - x^*_{N_2} = 1 - x_{H_2O,B} - x_{N_2,B} = x_{CO_2,B} + x_{O_2,B}$$

With no chemical reaction in the ash layer between the core and the flame front, the water conservation equation to be solved to obtain the key component profile will be

$$\nabla \cdot N_{H_2O} = 0$$

which after integration, $N_{H_2O} = -2Q_{H_2O}$ at $r = R_c$, yields

$$N_{H_2O} = -2Q_{H_2O}\frac{R_c^2}{r^2} \tag{24}$$

Substituting (24) into (23), we get

$$\nabla x_{H_2O} = -\frac{2}{\epsilon^2 cD}\left(\frac{x_{H_2O}}{2} - 1\right) Q_{H_2O}\frac{R_c^2}{r^2}$$

which now can be integrated knowing that $x_{H_2O} = x_{H_2O,B}$ at $r = R^*$ to yield

$$x_{H_2O} = 2 - (2 - x_{H_2O,B}) \exp\left[\frac{Q_{H_2O}R_c^2}{c\epsilon^2 D}\left(\frac{1}{r} - \frac{1}{R^*}\right)\right] \qquad R_c \leq r \leq R^* \tag{25}$$

$$x^c_{H_2O} = 2 - (2 - x_{H_2O,B}) \exp\left\{\frac{Q_{H_2O}R_c^2}{cD}\left[\frac{1}{\epsilon^2}\left(\frac{1}{R_c} - \frac{1}{R_p}\right) + \left(\frac{1}{R_p} - \frac{1}{R_\delta}\right)\right] - x_{O_2,B}\right\}, \quad R^* > R_c$$

If, however, $R^* = R_c$, then $x^c_{H_2O} = x_{H_2O,B}$

NUMERICAL RESULTS

To relate conditions in the bulk phase to those in the core, several options are available. In Table 4 it is seen that when all of the other bulk and core conditions are fixed, T_B, the bulk temperature, can be computed explicitly. Therefore, with R_c, R_p, R_δ, X, $x_{O_2,B}$, and $x_{H_2O,B}$ fixed as parameters, a curve in the T_c-T_B plane is obtained which indicates the achievable values of the core surface temperature for a given value of the temperature in the bulk phase. Such a plot will be used when a brief comparison between the homogeneous and inhomogeneous models is made. Alternatively, we can work in the $x_{O_2,B} - T_c$ plane. That is, by fixing R_c, R_p, R_δ, X, P, $x_{H_2O,B}$, and T_B as parameters, we can obtain a curve indicating the required oxygen concentration to achieve a given core temperature. If we now examine the expression for T_B corresponding to each location of the flame front, given in Table 4, we realize that they depend on the value of Q, the total rate of carbon consumption per unit area of core surface, defined in Equation (7).

$$x_{O_2,B} = \begin{cases} \dfrac{(T_B - T_c)\left\{1 + \dfrac{K_1 R_c^2}{cD}\left[\left(\dfrac{1}{R_p} - \dfrac{1}{R_\delta}\right) + \dfrac{1}{\epsilon^2}\left(\dfrac{1}{R_c} - \dfrac{1}{R_p}\right)\right]\right\}}{\Delta H_c R_c^2\left[\dfrac{1}{K}\left(\dfrac{1}{R_p} - \dfrac{1}{R_\delta}\right) + \dfrac{1}{K_e}\left(\dfrac{1}{R_c} - \dfrac{1}{R_\delta}\right)\right] K_1} - \dfrac{Q_{H_2O}}{K_1}, & R^* = R_c \quad (27a) \\ \dfrac{K_e}{cD\epsilon^2(\Delta H_c - \Delta H_I)}\left\{(T_B - T_c) - Q_{H_2O}R_c^2\left[\Delta H_c\left(\dfrac{1}{R_p} - \dfrac{1}{R_\delta}\right)\left(\dfrac{1}{K} - \dfrac{\epsilon^2}{K_e}\right) + \dfrac{\Delta H_I}{K_e}\left[\left(\dfrac{1}{R_c} - \dfrac{1}{R_p}\right) + \epsilon^2\left(\dfrac{1}{R_p} - \dfrac{1}{R_\delta}\right)\right]\right]\right\}, & R_c < R^* \leq R_p \quad (27b) \\ \dfrac{K}{cD(\Delta H_c - \Delta H_I)}\left\{(T_B - T_c) - Q_{H_2O}R_c^2\Delta H_I\left[\dfrac{1}{K}\left(\dfrac{1}{R_p} - \dfrac{1}{R_\delta}\right) + \dfrac{1}{K_e}\left(\dfrac{1}{R_c} - \dfrac{1}{R_p}\right)\right]\right\}, & R_p \leq R^* \leq R_\delta \quad (27c) \end{cases}$$

If the flame front is in the boundary layer, we must add the corresponding water conservation equation in the film together with the continuity conditions for concentration and flux at the particle surface:

$$x_{H_2O}|_{R_p^-} = x_{H_2O}|_{R_p^+}$$

$$N_{H_2O}|_{R_p^-} = x_{H_2O}|_{R_p^+}$$

If we integrate the resulting system of equations, the mole fraction profile in the ash layer turns out to be

$$x_{H_2O} = 2 - (2 - x_{H_2O,B}) \exp\left\{\frac{Q_{H_2O}R_c^2}{cD}\left[\frac{1}{R_p} - \frac{1}{R^*} + \frac{1}{\epsilon^2}\left(\frac{1}{r} - \frac{1}{R_p}\right)\right]\right\} \tag{26}$$

If the same value of D is used exterior to the flame, we can use Equations (8) and (9) to determine the radius of the reacting surface R^* and relate the water mole fraction in the core to the mole fractions of water and oxygen in the bulk. By doing so, both Equations (25) and (26) reduce to the same expression:

For the homogeneous model, once Q is substituted, we can solve for $x_{O_2,B}$ in terms of all the other variables, giving

For the heterogeneous model, since the steam mole fraction at the core (and consequently the steam gasification rate) is a nonlinear function of $x_{O_2,B}$ such an explicit solution is not possible, and therefore the T_B-T_c plot is more convenient. Each branch of Equation (27) is valid for a given region of the $x_{O_2,B}$-T_c plane, depending on the value of R^*. If we set $R^* = R_c$ in the expression given by Equation (8) for the flame front location when the flame front is within the ash layer, $x_{O_2,B}$ is obtained as

$$x_{O_2,B} = \left[\left(\frac{1}{R_c} - \frac{1}{R_p}\right)\frac{1}{\epsilon^2} + \left(\frac{1}{R_p} - \frac{1}{R_\delta}\right)\right]\frac{Q_{H_2O}R_c^2}{cD}$$

This is labeled B in Figure 4 and establishes a limit for flame separation from the core. The corresponding limit for flame separation from the particle (curve C in Figure 4) is obtained by setting $R^* = R_p$ in the equation for the flame front location when it is within the boundary layer [Equation (9)]. The resulting expression is

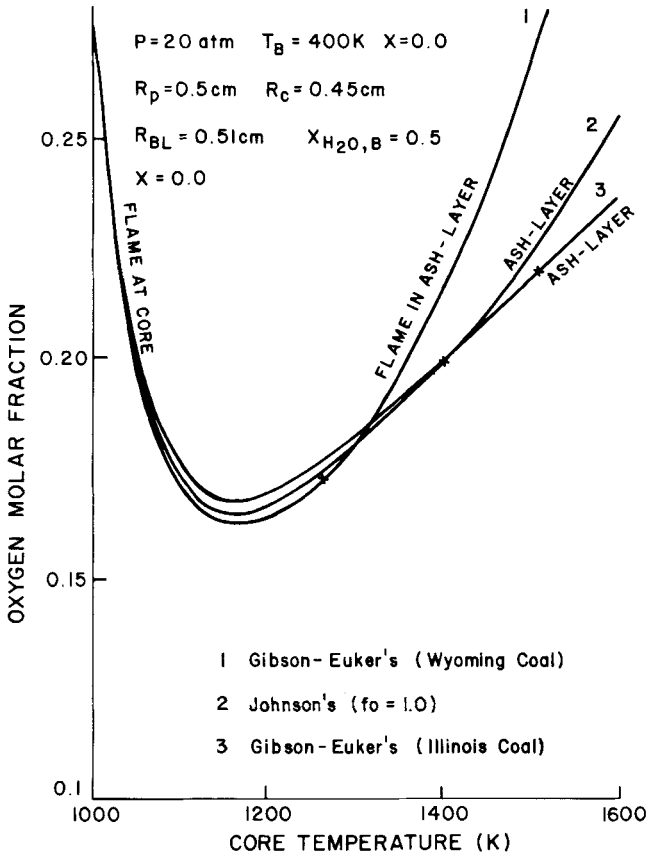

Fig. 5. Comparison of kinetic expressions. Ash layer present.

$$x_{O_2,B} = \left(\frac{1}{R_p} - \frac{1}{R_\delta}\right)\frac{Q_{H_2O}R_c^2}{cD}$$

These two curves divide the $x_{O_2,B}$-T_c plane into three regions: a region above curve B, where the flame front is always at the core external surface and Equation (27*a*) should be used; a region below curve C, where the flame front is always in the boundary layer and Equation (27*c*) should be used; and a region between curves B and C, where the flame front is always in the ash layer and Equation (27*b*) should be used. Plotting the corresponding branches (with the set of parameters indicated on Figure 4) we obtain curve A. At lower core temperatures, curve A bends down developing an additional branch not shown in the figure. The steady state multiplicity shown is of the type 1-3-5-3-1. For oxygen mole fractions in the gas phase below 0.0565 (point 7), the particle cannot be ignited, the only possible steady state being the one on the branch that is not shown and which corresponds to a very low core temperature. For $0.0565 \leq x_{O_2,B} \leq 0.077$ (point 5), three steady states are possible: extinction, ignition in the boundary layer, and ignition in the ash layer. For $0.077 \leq x_{O_2,B} \leq 0.083$ (point 6), the steady state multiplicity increases to five: extinction (in the branch not shown), ignition at the core surface (point 2), ignition in the boundary layer (point 4), and two intermediate states, one at the core surface (point 1) and one in the ash layer (point 3). Beyond $x_{O_2,B} = 0.083$, we have a three steady state situation until the limit $x_{O_2,B} = 0.10$ is reached. (We have assumed $x_{H_2O,B} = 0.9$ for our computations.) We will make some conjectures here about the solutions. In Figure 4 it should be noticed that when there are multiple solutions, say three (for ambient oxygen mole fractions above 0.083), the middle steady state corresponds to a flame front at the core surface. It is probably true that this is an unstable solution, so that aside from extinction, the only real steady state is with a flame front in the boundary layer. For ambient oxygen mole fractions between 0.077 and 0.083, there are five solutions as mentioned above, and one of those at the core surface is probably unstable as well as the one on the ash layer. In this case the three stable states are probably, aside from extinction, one with a flame front at the core surface and the other in the boundary layer.

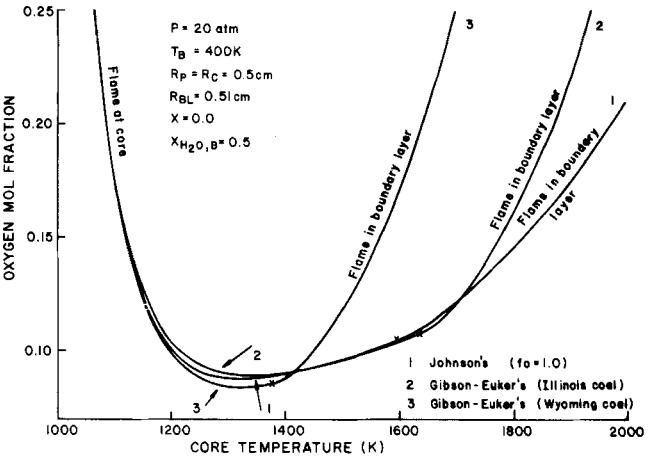

Fig. 6. Comparison of kinetic expressions. No ash layer.

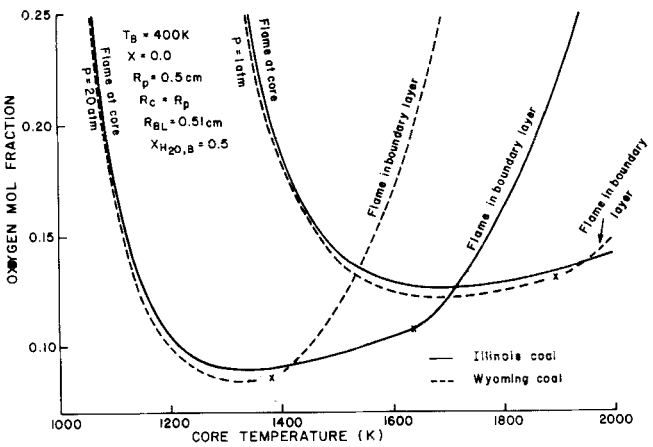

Fig. 7. Effect of changes in pressure (Gibson-Euker kinetic expressions).

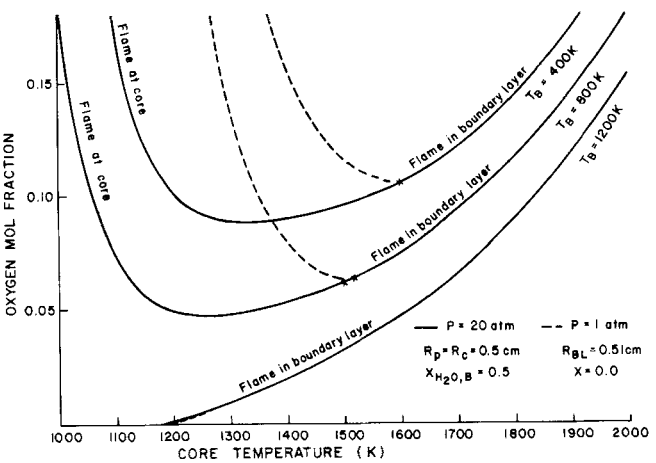

Fig. 8. Effect of changes in pressure and in bulk temperature [Johnson kinetic expression (f_o = 1.0)].

These are fairly widely separated in core temperature, and the one obtained would depend upon the start-up condition. Below ambient oxygen mole fraction of 0.077 but above 0.0565, the real steady state solution is probably the one with a flame front in the boundary layer. Below 0.0565 there is only extinction.

Effect of the Form of the Reaction Rate Expressions

In Figures 5 and 6 comparisons were made for different kinetic expressions. For Johnson's model a relative reactivity factor f_o of 1 was assumed. Figure 5 shows results when there is an ash layer 0.05 cm thick, while no ash layer was assumed to exist for computations shown in Figure 6. Otherwise, all of the parameters used were the same in both cases, and their values are shown on the graphs. Observe that in these figures the curves representing the limits for separation of flame either from the core or particle (curves B and C of Figure 4) are omitted; only their intercepts with the main curve are shown by crosses. This procedure will be followed for all of the plots. For relatively low core temperatures (below 1 200°K), there is no significant deviation among the curves. This is a natural consequence of the fact that under these conditions the flame front is at the core surface, and therefore the important reaction is the direct combustion of carbon. Therefore, $Q_{H_2O} << K_1$, and the second term on the right-hand side of Equation (27*a*) is negligible when compared with the first resulting in an expression for $x_{O_2,B}$ which is independent of the type of kinetics assumed for the steam gasification reaction. At higher core temperatures, the flame separates from the core surface, and either Equation (27*b*) or (27*c*) is applicable. These are strongly dependent on Q_{H_2O}. A higher reactivity coal (Wyoming coal) will then produce a curve which lies above the others, because by gasifying more carbon by reaction with steam, more heat must be provided by a larger oxygen consumption in the flame, and, therefore, a larger oxygen mole fraction is required in the gas phase. Johnson's kinetics and Gibson-Euker's for Illinois coal do not produce significantly different results up to temperatures as high as 1 700°K, although flame separation from the core surface has already occurred. Beyond that point, the curves start diverging, but by then we are exceeding the range of validity of those empirical expressions. Therefore, the two models are roughly equivalent.

Effect of Changes in Pressure

In Figures 7 and 8 the qualitative influence of changes in pressure at a low core temperature is the same for both kinetic models; namely, an increase in pressure implies a decrease in the mole fraction of oxygen permitted because the dominant process is the direct combustion of carbon and, therefore, an increase in pressure implies an increase of heat generation in the core. The behavior at high core temperatures is, however, strongly dependent on the kinetic model assumed. Johnson's model (Figure 8) will predict that the oxygen mole fraction in the bulk, when the flame is in the film, is independent of pressure. Gibson-Euker's, on the other hand, predicts that an increase in $x_{O_2,B}$ follows an increase in pressure. This follows from the fact that Johnson's model, while being second order in p_{H_2O} at low core temperatures, becomes of order zero at high temperatures and therefore, under those conditions, is pressure independent. Gibson-Euker's model, on the contrary, is always first order in p_{H_2O}. We can also observe that according to Gibson-Euker's model the flame separation from the core must occur at a lower core temperature for higher pressures because of the larger rate of steam gasification, while Johnson's will predict that such

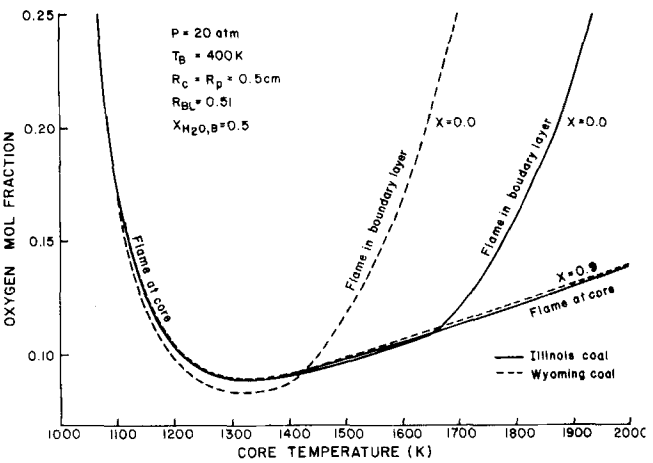

Fig. 9. Effect of changes in core conversion (Gibson-Euker kinetic expression).

a separation point is quite insensitive to changes in pressure because it occurs at core temperatures where Q_{H_2O} has already almost zero-order dependency on the steam partial pressure and consequently on the pressure. The effect of changes in steam concentration is equivalent to the effect of changes in total pressure, and therefore this need not be discussed.

Effect of Changes in Core Conversion

This effect is shown for both models in Figures 9 and 10. A lower core conversion implies a larger reaction rate for steam gasification, and we have to expect that there will be no sensible effect at low core temperature when the predominant process is the direct carbon com-

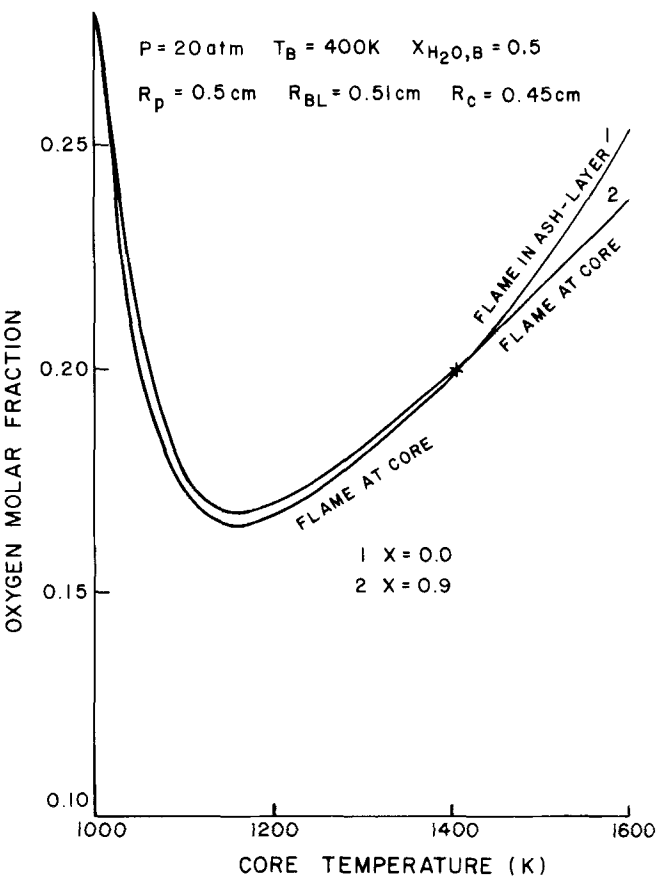

Fig. 10. Effect of changes in core conversion [Johnson kinetic expression (f_o = 1.0)].

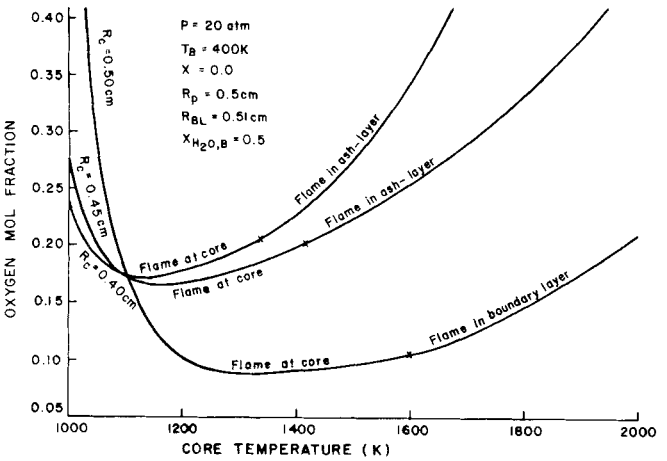

Fig. 11. Effect of changes in bulk temperature (Gibson-Euker kinetic expression for Illinois coal).

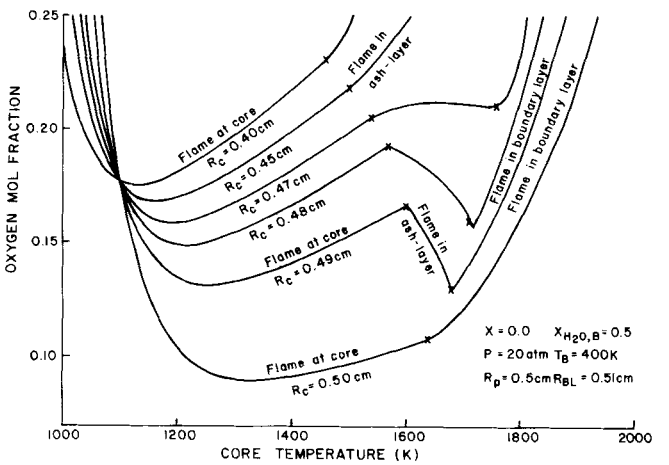

Fig. 13. Effect of changes in core radius (Gibson-Euker kinetic expression for Illinois coal).

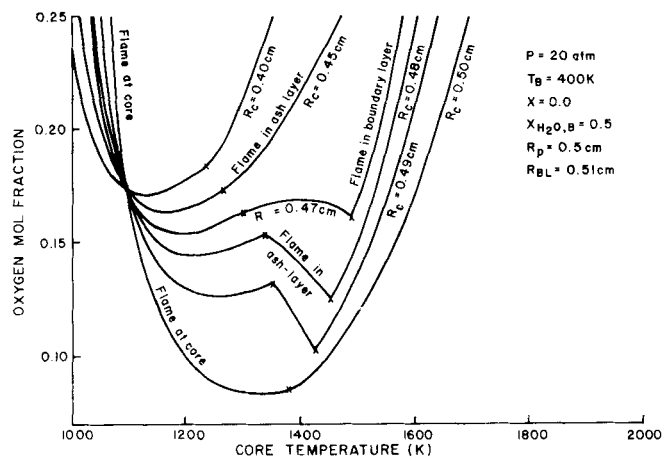

Fig. 12. Effect of changes in core radius (Gibson-Euker kinetic expression for Wyoming coal).

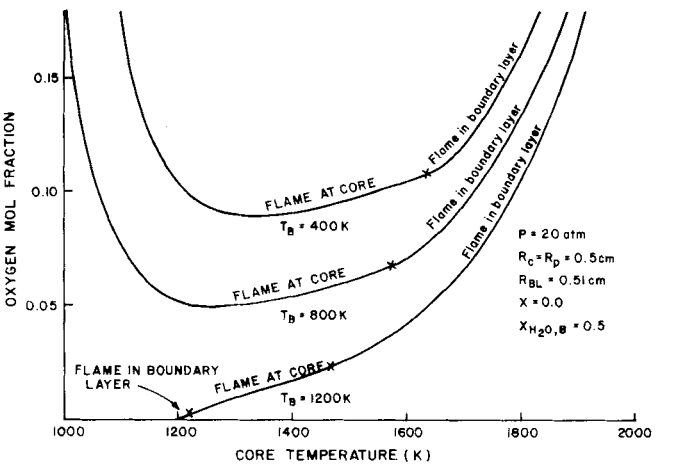

Fig. 14. Effect of changes in core radius [Johnson kinetic expression (f_O = 1.0)].

bustion, a higher oxygen mole fraction in the bulk phase required to provide by combustion in the flame the necessary heat to compensate for the increased consumption of heat in the core by the enhanced endothermic steam gasification, and a flame separation from the core surface at lower temperatures. All these effects are shown in the indicated graphs.

Effect of Changes in Bulk Temperature

When the flame is at the core surface, the effect of lowering the temperature of the gas phase can be visualized by considering that more of the heat generated at the core can be released, and consequently a larger oxygen mole fraction is permitted. If the flame is away from the core surface, a lower bulk temperature will require a larger $x_{O_2,B}$ to insure enough heat to compensate for the amount absorbed by the endothermic reaction. The net effect is an upward shift of the curves for lower T_B values. Such an effect is shown in Figure 11 for Illinois coal (Gibson-Euker's model) and in Figure 8 for Johnson's.

Effect of Changes in Core Radius

The qualitative effect of changes in core radius is shown in Figures 12, 13, and 14. Observe that an increase in the admissible mole fraction of oxygen is predicted for increasing core radius at relatively low temperatures, while the opposite is true for larger values of T_c. A larger value for R_c produces two different effects: to increase the reaction rate by enlarging the available area and to reduce the resistance to heat and mass transfer by diminishing the thickness of the ash layer. At a low temperature, when negligible reaction occurs, the increase of the area is not as important a factor as the decreased resistance to heat release. By increasing the core temperature, the phenomenon starts to reverse itself and is completed at about 1 100°K. The reaction rate has increased, and it is now significant. Smaller cores by implying not only less reactive surface but also increased resistance to oxygen diffusion will permit larger oxygen concentrations in the bulk phase. When the flame separates from the core, the increased resistance to both heat and mass flow requires a larger oxygen consumption in the flame and therefore a larger value for the oxygen mole fraction in the bulk.

Comparison between Homogeneous and Heterogeneous Models

The heterogeneous model by including a resistance to the steam diffusion from the flame to the core surface will affect the steam gasification rate. The comparison will be made using Johnson's kinetics for which if the flame separates from core at sufficiently high T_c, the difference between models should be negligible. This flame separation at high core temperatures is insured by setting a core conversion value $X = 0.8$ which represents a typical combustion zone value for the Lurgi gasifier. Observe in Figure 15 that the two curves can

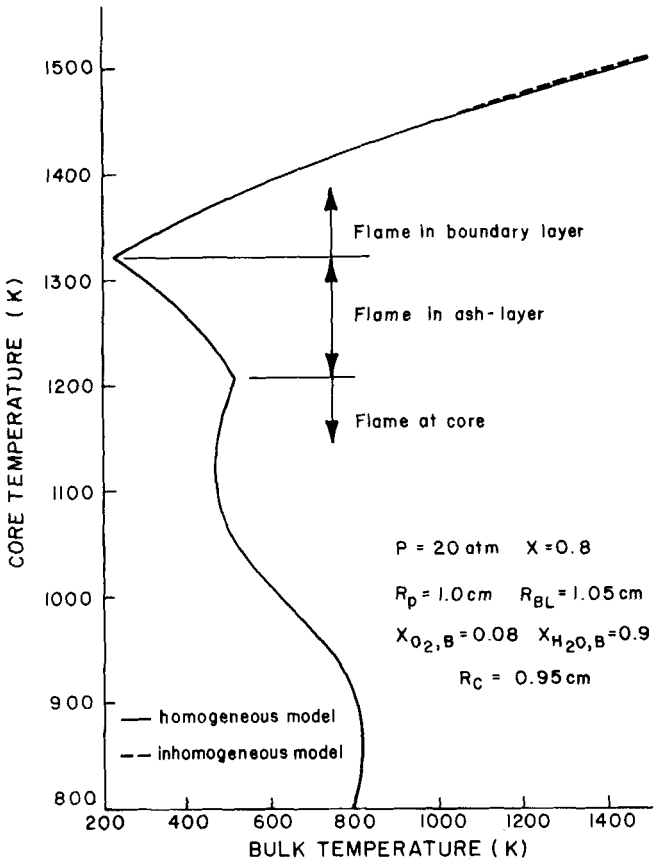

Fig. 15. Model comparison when flame separates from core at high core temperature [Johnson kinetic expression ($f_o = 1.0$)].

barely be distinguished, and for core temperature as high as 1 470°K the homogeneous model predicts a required bulk temperature less than 2 °K higher than the one predicted considering mass transfer resistance between core and flame surface. Observe also that for a less reacted

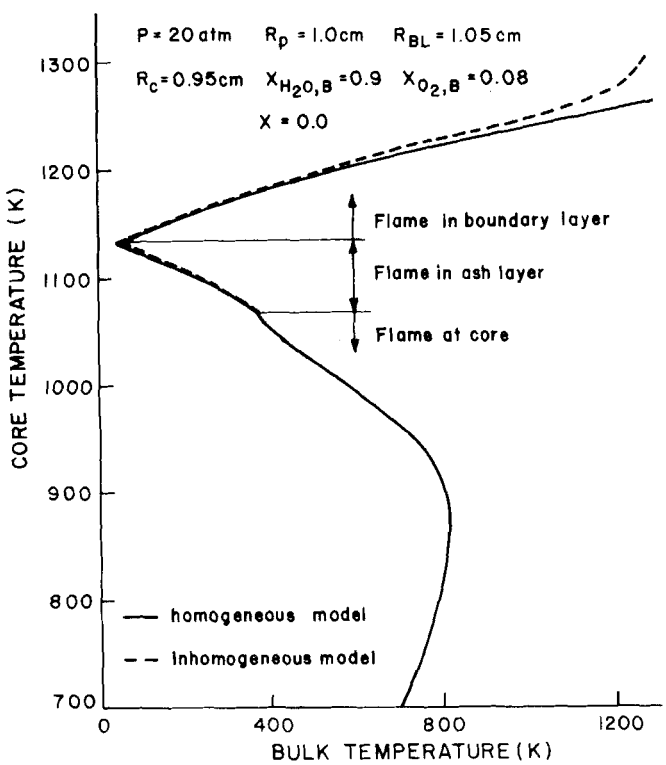

Fig. 16. Model comparison when flame separates from core at low core temperature [Johnson kinetic expression ($f_o = 1.0$)].

core ($X = 0$ in Figure 16) for values of the core temperature up to 1 250°K there is no significant difference between models, but beyond that point the two curves begin to differ widely, the homogeneous model requiring a much larger bulk temperature.

ACKNOWLEDGMENT

This work was not supported by any alphabetical agency, either public or private, except the University of Minnesota (whom we applaud).

NOTATION

a_i = relation between stoichiometric coefficients for the reaction $C + 2H_2O \rightarrow CO_2 + 2H_2$ used in the heterogeneous model
C_{pi} = molar heat capacity of the i^{th} gas component
c = total molar concentration
D = diffusivity
D_e = effective diffusivity in the particle ash layer
D_H = binary diffusivity of any species in hydrogen
D_{ij} = binary diffusivity
f_o = relative reactivity factor
f_L = reactivity factor defined in Table 1*a*
h_i = partial molar enthalpy of i^{th} component
K = gas conductivity
K_e = effective conductivity of the ash layer in the particle
K_i = specific rate of the i^{th} reaction
K_I^{eq} = equilibrium constant of the reaction $C + H_2O \rightarrow CO + H_2$
K_{II}^{eq} = equilibrium constant of the reaction $C + 2H_2 \rightarrow CH_4$
K_{III}^{eq} = equilibrium constant of the reaction $2C + H_2O + H_2 \rightarrow CH_4 + CO$
k_i = individual rate constants for each of the individual reactions in IGT scheme
k_T = global rate constant in IGT scheme
M_c = carbon molecular weight
N_i = molar flux of the i^{th} component
P = pressure
p_i = partial pressure of the i^{th} component
Q = total rate of carbon consumption per unit area of core surface
Q_{H_2O} = total rate of carbon consumption due to steam and carbon dioxide gasification per unit area of core surface
q = heat flux
R_c = core redius
R_p = particle radius
R_δ = radius at the outer edge of boundary layer
R^* = flame surface radius
r = radial coordinate
T = temperature
T_B = bulk temperature
T_c = core temperature
X = solid conversion referred to the fixed carbon
x_i = molar fraction of i^{th} gaseous component
$x_{i,B}$ = molar fraction of i^{th} gaseous component in the bulk
x_i^c = molar fraction of i^{th} gaseous component at core surface

Greek Letters

α = function defined in Table 1*a*
α_i = stoichiometric coefficient of i^{th} species in the reaction $C + 2H_2O \rightarrow CO_2 + H_2$
α_I = combination of variables used in Table 3 ($Q\Delta C_{pI}R_c^2/K$)
α_{II} = combination of variables used in Table 3 ($Q\Delta C_{pII}R_c^2/K$)

α_{eI} = combination of variables used in Table 3 $(Q\Delta C_{pi}R_c^2/K_e)$
α_{eII} = combination of variables used in Table 3 $(Q\Delta C_{pII}R_c^2/K_e)$
ΔC_{pI} = combination of C_{pi}'s
ΔC_{pII} = combination of C_{pi}'s
ΔH_c = enthalpy change for the reaction $C + O_2 \rightarrow CO_2$
ΔH_w = enthalpy change for the reaction $H_2 + \frac{1}{2}O_2 \rightarrow H_2O$
ΔH_I = enthalpy change for the reaction $C + 2H_2O \rightarrow CO_2 + 2H_2$
ϵ = ash layer porosity
ρ_{CF} = mass of fixed carbon per unit unreacted particle volume conditions

Subscript

B = condition in the bulk phase
c = condition at the core surface

Superscript

c = condition at the core surface

LITERATURE CITED

Arthur, J. R., "Reactions Between Carbon and Oxygen," *Trans. Faraday Soc.*, **47**, 164 (1951).

Burke, S. P., and T. E. W. Schumam, "The Mechanism of Combustion of Solid Fuel," *Proc. 3rd Intern. Conf. Bituminous Coal*, **2**, 485 (1931).

Blackwood, J. D., "The Kinetics of the System Carbon-Hydrogen-Methane," *Aust. J. Chem.*, **15**, 397 (1962).

———, and D. J. McCarthy, "The Mechanism of Hydrogenation of Coal to Methane," *ibid.*, **19**, 797 (1966).

Blackwood, J. D., and F. McGrory, "The Carbon-Steam Reaction at High Pressure," *ibid.*, **11**, 16 (1958).

Caram, H., and N. R. Amundson, "Diffusion and Reaction in a Stagnant Boundary Layer About a Carbon Particle," *Ind. Eng. Chem. Fundamentals*, **16**, No. 2, 171 (1977).

Gibson, M. A., and C. A. Euker, Jr., "Mathematical Modeling of Fluidized Bed Coal Gasification," preprint presented at AIChE Symposium on Laboratory Reactors, Los Angeles, Calif. (Nov., 1975).

Field, M. A., D. W. Gill, B. B. Morgan, and P. G. W. Hawksley, "Combustion of Pulverized Coal," The British Coal Utilization Research Association, Leatherhead (1967).

Institute of Gas Technology, "Production of Pipeline Gas by Hydrogasification of Coal," *Res. Bull. No. 39*, 1 (1972).

Johnson, J. L., "Kinetics of Bituminous Coal Char Gasification with Gases Containing Steam and Hydrogen," *Adv. Chem. Ser.*, 131, ACS (1974).

Spalding, D. B., *Some Fundamentals of Combustion*, Butterworths, London, England (1955).

van der Held, E. F. M., "The Reaction Between a Surface of Solid Carbon and Oxygen," *Chem. Eng. Sci.*, **14**, 300 (1961).

Wen, C. Y. and S. C. Wang, "Thermal and Diffusional Effects in Non-Catalytic Solid Gas Reactions," *Ind. Eng. Chem.*, **62**, No. 8, 30 (1970).

Wen, C. Y., and J. Huebler, "Kinetic Study of Coal Char Hydrogasification. Rapid Initial Rate," *Ind. Eng. Chem. Process Design Develop.*, **4**, 142 (1965).

———, "Kinetic Study of Coal Char Hydrogasification. Second-Phase Reaction," *ibid.*, 147 (1965).

Wicke, E., and G. Wurzbacher, "Konzentrationsprofile vor einer im Sauerstoffstrom verbrennenden hohlenstoffoberfläche I.," *Intern. J. Heat Mass Transfer*, **5**, 277 (1962).

Manuscript received May 13, 1977; revision received and accepted August 23, 1977.

Char Gasification in a Countercurrent Reactor

NEAL R. AMUNDSON
and
LUIS ERNESTO ARRI

Department of Chemical Engineering and Materials Science
University of Minnesota
Minneapolis, Minnesota 55455

A model is developed for the countercurrent char gasifier of Lurgi form. Char particles are fed to the top and oxygen, inert, and steam in the bottom. The combustion zone is defined as the zone in which there is a nonzero molfraction of oxygen. In the gasification zone, the particles are assumed to be a lumped system in which the Johnson reaction kinetic expressions are assumed to be valid with the water gas shift reaction at equilibrium. All of the reactions between oxygen and carbon and water and carbon are assumed to take place in the combustion zone but with the carbon-oxygen reaction predominating to form a shell progressive system within the particles. Radiation is taken into account, and parametric computations are made on temperatures, compositions, flow rates, and char reactivity. The maximum temperature is strongly influenced by radiation and its position is a sensitive function of the solid flow rate producing an ash layer at the bottom of varying thickness.

SCOPE

The purpose of this study was to develop a model for a countercurrent moving-bed gasifier of coal, actually char, which would predict at least qualitatively the known features of such systems. There has been little modeling with this system, although the general subject of gas-solid reactions in moving beds has been examined in detail, notably by Ishida and Wen (1971) and Wen and Wang (1970). A quantitative model of the countercurrent gasifier was presented by Yoon et al. (1976), and there have been numerous descriptive and qualitative discussions by Elgin and Perks (1973, 1974), Rudolph (1974), Hebden (1975), and Hoogendorn (1973). In addition, Woodmansee (1975) updated some very early models. There is almost no real operating information available in the literature, and one

Neal R. Amundson is at the University of Houston, Houston, Texas 77004. Luis Ernesto Arri is with INTEC (U.N.L-CONICET), Santiago del Estero 2654, 3000 Santa Fé, Argentina.